


## Investigation of the Stark Effect on a Centrosymmetric Quantum Emitter in Diamond

Lorenzo De Santis<sup>1,2,†</sup>, Matthew E. Trusheim<sup>1,3</sup>, Kevin C. Chen<sup>1</sup>, and Dirk R. Englund<sup>1,\*</sup>

<sup>1</sup>*Department of Electrical Engineering and Computer Science, Massachusetts Institute of Technology, Cambridge, Massachusetts 02139, USA*

<sup>2</sup>*QuTech, Delft University of Technology, PO Box 5046, 2600 GA Delft, Netherlands*

<sup>3</sup>*CCDC Army Research Laboratory, Adelphi, Maryland 20783, USA*

 (Received 5 February 2021; accepted 23 August 2021; published 28 September 2021)

Quantum emitters in diamond are leading optically accessible solid-state qubits. Among these, Group IV-vacancy defect centers have attracted great interest as coherent and stable optical interfaces to long-lived spin states. Theory indicates that their inversion symmetry provides first-order insensitivity to stray electric fields, a common limitation for optical coherence in any host material. Here we experimentally quantify this electric field dependence via an external electric field applied to individual tin-vacancy (SnV) centers in diamond. These measurements reveal that the permanent electric dipole moment and polarizability are at least 4 orders of magnitude smaller than for the diamond nitrogen vacancy (NV) centers, representing the first direct measurement of the inversion symmetry protection of a Group IV defect in diamond. Moreover, we show that by modulating the electric-field-induced dipole we can use the SnV as a nanoscale probe of local electric field noise, and we employ this technique to highlight the effect of spectral diffusion on the SnV.

DOI: [10.1103/PhysRevLett.127.147402](https://doi.org/10.1103/PhysRevLett.127.147402)

Quantum emitters in diamond have emerged as leading solid-state quantum memories. The nitrogen vacancy (NV) center, in particular, has been used for basic quantum network demonstrations [1,2] including on-demand entanglement [3]. Despite the NV's excellent spin properties, its optical interface is inefficient: only a small fraction of emission occurs into the spin-correlated zero-phonon line (ZPL) [4]. Integration into photonic nanostructures can improve this branching ratio, but at the cost of spectral diffusion because of the NV's sensitivity to electric field fluctuations, particularly strong near material interfaces [5,6]. These challenges have sparked interest towards inversion-symmetric group IV-vacancy quantum emitters (SiV, GeV, SnV, and PbV), whose ZPL emission fraction can be an order of magnitude greater than in the NV. Additionally, these emitters showed low spectral diffusion and lifetime-limited emission even in nanostructures [7]. Such robustness is attributed to their  $D_{3d}$  symmetry, which has been predicted to produce a first order insensitivity to electric fields [8]. This property enabled the demonstration of high QED cooperativities for cavity-coupled emitters [9], wide spectral tuning of their emission energies [10], and large-scale integration of defects in waveguides [11]. Despite being one of its key advantages, no measurement of the first-order electric field insensitivity of a group IV emitter has been reported to date. In this work, we directly test the expected insensitivity to electric fields by investigating the Stark effect on a single SnV emitter. We confirm the absence of a significant permanent electric dipole moment, as well as an extremely low

polarizability—orders of magnitude lower than for the NV center. Finally, we use the electric-field-induced dipole of the SnV defect as a nanoscale probe to estimate the electric field noise in its vicinity.

We consider the negatively charged SnV in diamond as a prototypical group-IV emitter. They share qualitatively identical electronic structure consisting of four electronic orbitals, two for the excited and two for the ground state, connected by four optical transitions [8]. The  $D_{3d}$  symmetry that gives rise to the predicted first-order insensitivity is preserved [12–14]. Moreover, the large ground-state orbital splitting of the SnV (850 GHz for SnV compared to 50 GHz for SiV) gives it the potential for long spin coherence above dilution refrigerator temperatures, a key consideration for use as a quantum memory [15,16].

The SnV emitters analyzed here are created in a CVD-grown type IIa diamond through ion implantation. An interdigitated electrode structure on the surface allows us to apply an electric field aligned with the crystalline [110] axis as depicted in Fig. 1(a) with negligible leakage current (details in the Supplemental Material [17]). Optical characterization is performed using a confocal setup, with a sample temperature of 4 K. A spatial photoluminescence (PL) emission map obtained with a 515 nm pump laser is shown in Fig. 1(b), and the emission spectrum in Fig. 1(c). The spectrum originates from an ensemble of emitters within the optical diffraction limit, and shows the two SnV transitions active at this temperature. We focus here on the higher-energy emission line, which is the optical interface to the long-lived lower ground state of the SnV [16]. To

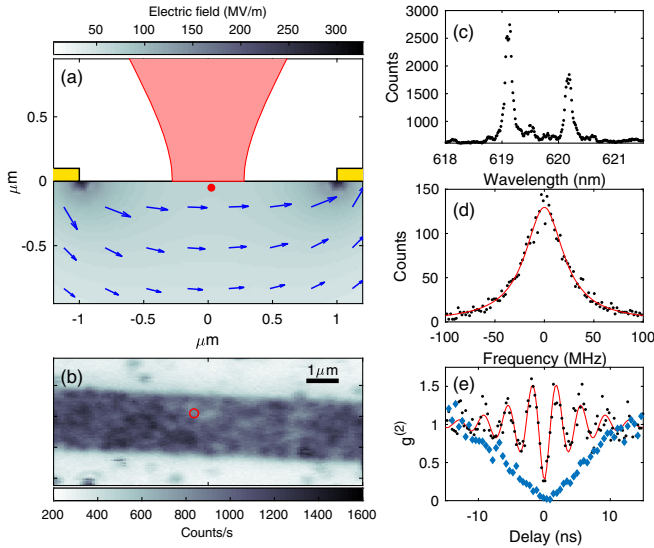


FIG. 1. (a) Side view of the sample layout, showing two gold electrodes and the electric field distribution simulated with COMSOL for an external bias of 200 V. A red circle indicates the emitter location (76 nm below the surface). (b) Confocal PL scan of the sample, showing an ensemble of emitters in the exposed diamond, enclosed between two electrodes. The red circle locates the SnV emitter analyzed here. (c) Typical emission spectrum obtained under non-resonant excitation. (d) PLE spectrum of the transition to the lower ground state of an SnV, showing a linewidth of 47 MHz. (e) Second order correlation measurement performed under weak (blue diamonds) and strong driving (black dots).

investigate single SnV defects, we use photoluminescence excitation (PLE), by scanning the frequency of a narrow-band laser across the emitter's ZPL while detecting the phonon sideband emission. Figure 1(d) plots the result of a PLE measurement performed in the weak excitation regime, from which we can extract a single-transition linewidth of  $47 \pm 2$  MHz. By fixing the excitation laser on resonance with the transition, we perform a second-order correlation measurement as shown in Fig. 1(e). At low excitation power we obtain a value of  $g^{(2)}(0) = 0.03$ , confirming the single-photon nature of the emission, and an optical  $T_1$  lifetime of  $6.0 \pm 0.5$  ns corresponding to a lifetime-limited linewidth of  $27 \pm 2$  MHz. Under strong driving, the  $g^{(2)}$  measurement reveals Rabi oscillations with a phase lifetime  $T_2$  of  $4.0 \pm 0.5$  ns ( $40 \pm 4$  MHz).

The effect of a static electric field on the energy of an atomlike transition is the well-known dc Stark effect. It results in an energy shift of the transition which depends on the difference  $\Delta\mu_{\text{ind}}$  between the excited and ground state dipole moments, and can be expanded as a power series in the electric field  $F$  [18]. Conventionally, Stark shift measurements focus on linear and quadratic shifts, and have been extensively used to investigate the polarizabilities of atoms and molecules [19,20]. Here we consider

shifts up to the fourth order in  $F$ , giving an expected SnV transition energy shift  $\Delta E$  of

$$\Delta E = -\Delta\mu_{\text{ind}}(F)F = -\Delta\mu F - \frac{1}{2}\Delta\alpha F^2 - \frac{1}{3!}\Delta\beta F^3 - \frac{1}{4!}\Delta\gamma F^4. \quad (1)$$

The first two terms of this equation allow us to extract the difference between the ground and excited orbital states in permanent dipole moment  $\Delta\mu$  and in polarizability  $\Delta\alpha$ , while the terms  $\Delta\beta$  and  $\Delta\gamma$  are related to the differences in the second and third order hyperpolarizabilities of the electronic states. Using standard perturbation theory, the first-order Stark shift on the  $i$ th orbital is given by the matrix element  $\langle\psi_i|\mu|\psi_i\rangle$ , where  $\mu$  is the electric dipole operator, an odd function of position. Since the two SnV ground (excited) state orbitals maintain even (odd) symmetry, these matrix elements should vanish. The second-order correction is given by  $\sum_{j \neq i} [|\langle\psi_i|\mu|\psi_j\rangle|^2 / (E_i - E_j)]$ . The only contributions to this sum are due to the matrix elements connecting ground and excited states, which should contribute little due to their large energy separation. We thus expect both the first- and second-order Stark shifts to be strongly suppressed in an ideal crystal.

We approximate the local electric field  $F$  acting on the defect from the Lorentz local field approximation [21]  $F = F_{\text{ext}}(\epsilon + 2)/3$ , where  $F_{\text{ext}}$  is the externally applied field, extracted from the COMSOL simulation of Fig. 1(a), and  $\epsilon$  the dielectric constant of diamond. Owing to the charge stability of the defect and the high dielectric strength of diamond, we can apply electric fields exceeding 200 MV/m and thereby detect even weak Stark effects. Figure 2(a) presents the PLE measurements, revealing the dependence of the SnV absorption spectrum on the electric field  $F$ . Such dependence shows a nonlinear Stark shift, a direct consequence of the absence of a permanent electric dipole. The black dots in Fig. 2(b) indicates the frequency shift in the transition of the SnV emitter, determined by fitting to the PLE spectrum. For this emitter, we extract a linear shift with a slope of  $6.1 \times 10^{-4}$  GHz/(MV/m), corresponding to a difference in dipole moment of  $\Delta\mu = 1.2 \pm 0.2 \times 10^{-4}$  D. From the same fit, we can also extract a quadratic shift coefficient of  $-5.1 \times 10^{-5}$  GHz/(MV/m)<sup>2</sup>, corresponding to a polarizability difference of  $\Delta\alpha = 0.31 \pm 0.01 \text{ \AA}^3$ .

Figure 3 reports the measured Stark coefficients of 12 individual SnV centers, showing the observed change in dipole moment as a function of the change in polarizability. The resulting distribution of  $\Delta\mu$  shows a mean of  $0.4 \times 10^{-4}$  D and standard deviation of  $3.9 \times 10^{-4}$  D, compatible with the expected absence of a permanent SnV electric dipole. The polarizability differences  $\Delta\alpha$  are instead always positive, with a mean and standard deviation, respectively, of 0.23 and 0.13  $\text{\AA}^3$ . The variability of these parameters

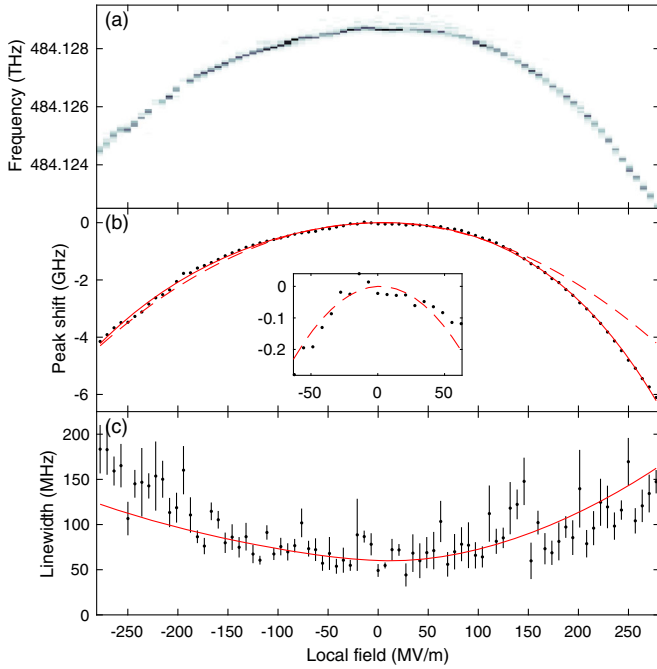


FIG. 2. (a) PLE spectra as a function of the local electric field at the defect. (b) Shift of the center position of the transition (black dots). The dashed and solid red lines show a fit to a second and a fourth order polynomial, respectively. The inset is a close up of the shift for small applied fields, where the behavior is quadratic. (c) Linewidth of the emitter showing a broadening of the transition.

originates from the local environment of each emitter: strain fields, which are also visible in the emitters' inhomogeneous distribution [22], and residual electric fields, known to induce linear dipole on single molecule systems [23,24], can locally affect the orbitals of the SnVs. Nonetheless, we measure values of  $\Delta\mu$  and  $\Delta\alpha$  that are 4 orders of magnitude smaller than those reported for the Stark shift of NV centers [25,26]. This observation supports the inversion symmetry protection of group IV-vacancy

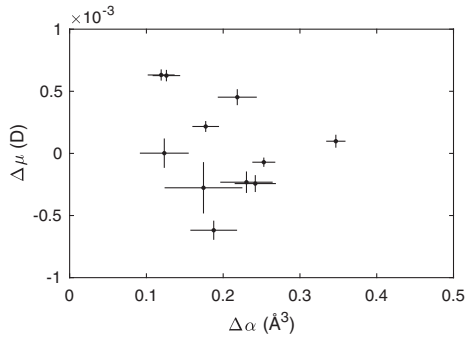


FIG. 3. Experimental values of the change in dipole moment ( $\Delta\mu$ ) versus the change in polarizability ( $\Delta\alpha$ ) for different SnV centers. The average polarizability is  $0.23 \text{ \AA}^3$ , while the average dipole moment is  $0.4 \times 10^{-4} \text{ D}$ .

centers, showing that the exceptional electric field insensitivity arises both from the limited permanent electric dipole as well as a low polarizability. At the same time, each emitter exhibits a Stark shift of at least 1 GHz, which corresponds to a tuning range more than 37 times larger than their natural linewidth, without any noticeable quenching of emission intensity. Electric fields can thus be used for the spectral tuning of the transition frequency of group IV color centers without noticeable degradation of optical properties.

The lack of a permanent dipole and low polarizability, however, is not adequate to describe the Stark shifts at high fields ( $> 100 \text{ MV/m}$ ) where higher-order corrections (hyperpolarization) become significant. The observed dependence including these contributions is well reproduced by a fourth-order description (solid red line), showing a fit to Equation (1). The third and fourth order coefficients are, respectively,  $-5.5 \pm 0.3 \times 10^{-8} \text{ GHz}/(\text{MV/m})^3$  and  $-2.2 \pm 0.2 \times 10^{-10} \text{ GHz}/(\text{MV/m})^4$ , whose total contribution to the observed spectral trajectory is up to 25%. These higher-order effects, linked to higher-order moments of the optical transition [18], have been observed in systems such as molecules [27] and hydrogenlike atoms, where only even-order terms are present due to their symmetry [28]. This study shows that centrosymmetric defects in diamond such as the SnV enable the observation and control of hyperpolarization effects solid state systems.

To extend the analysis above, we also investigate the effect of the applied electric field on the emitter linewidth. We fit the PLE measurements of Fig. 2(a) to a pseudo-Voigt profile, and extract the SnV linewidth as shown by the black dots in Fig. 2(c). In these measurements the laser scan across the transition in 2.5 s, thus they include all dephasing and spectral diffusion effects happening up to that timescale. Without an external field, the emitter shows a narrow linewidth of  $49 \pm 7 \text{ MHz}$ , which is a factor of 1.7 above the lifetime limit of 27 MHz. For higher fields, however, a considerable broadening occurs regardless of polarity, increasing the linewidth up to 150 MHz. We attribute this behavior to the increased sensitivity of the SnV center to charge noise in its surroundings. A higher value of a static external field  $F_{\text{dc}}$  will induce a higher dipole on the defect, thus a same field fluctuation will shift the optical transition further. We assume here a root mean square electric field noise at the defect location having a fixed magnitude  $F_{\text{r.m.s}} \ll F_{\text{dc}}$ . By replacing  $F = F_{\text{dc}} + F_{\text{r.m.s}}$  in Equation (1), we see that  $F_{\text{r.m.s}}$  will produce a root mean square line shift of  $\sigma_G = \Delta\mu_{\text{ind}}(F_{\text{dc}})F_{\text{r.m.s}}$ . This results in a Voigt absorption line shape on the emitter, which can be related to the constituent Lorentzian and Gaussian width as  $\Gamma_V = (\Gamma_L/2) + \sqrt{(\Gamma_L/2)^2 + \Gamma_G^2}$  [29]. We identify here  $\Gamma_L$  as the homogeneous linewidth of the SnV emitter, while  $\Gamma_G = 2\sqrt{2} \ln 2 \sigma_G$  describes the stochastic Stark shift due to  $F_{\text{r.m.s}}$ . The expected SnV linewidth can then be modeled as

$$\Gamma = \frac{\Gamma_L}{2} + \sqrt{\left(\frac{\Gamma_L}{2}\right)^2 + 8 \ln 2 [F_{r.m.s} \Delta\mu_{ind}(F_{dc})]^2}, \quad (2)$$

where  $\Delta\mu_{ind}(F_{dc})$  can be deduced from the Stark shift analysis of the previous section. We fit this equation to the measured linewidth values as shown in the red line of Fig. 2(c), from which we extract an average field fluctuation of  $F_{r.m.s} = 2.4 \pm 0.2$  MV/m as well as a minimum linewidth of  $\Gamma_L = 60 \pm 4$  MHz. Although this measured  $F_{r.m.s}$  is over 4 orders of magnitude greater than reports for InGaAs QD devices [30], the SnV emitters still show linewidths close to the lifetime limit, highlighting again their insensitivity to the charge environment. We note moreover that for  $F_{dc} = 0$  the extracted field fluctuation  $F_{r.m.s}$  produces an average Stark shift much smaller than the natural linewidth of the SnV, thus the residual broadening above the lifetime limit should not be associated with electric field noise.

We also investigated short-time SnV optical dynamics by fast sweeps of the PLE excitation laser at a rate of 20 GHz/s, scanning across the SnV transition in 1.3 ms. At each bias value, the PLE scans are repeated multiple times to produce temporal series as in Figs. 4(a) and 4(b). These measurements reveal a narrow and stable transition at zero bias field [Fig. 4(a)], while an increasingly strong spectral diffusion appears with larger electric fields [Fig. 4(b)]. The mean of the PLE linewidths from individual high-speed scans as a function of the electric field is shown by the black dots in Fig. 4(c). In contrast to the observations of Fig. 2(c), the linewidth measured at this timescale is consistent with a zero-bias value of 45 MHz: it does not significantly depend on the applied field. The broadening effect can instead be reproduced from the standard deviation of the peak positions in a temporal series, as seen in the blue diamonds in Fig. 4(c). These data confirm our attribution of the SnV linewidth broadening to the electric-field dependent SnV dipole moment  $\Delta\mu_{ind}(F)$ , which is responsible for the stochastic Stark shift observed in Fig. 4(b). Moreover, we can confirm that this effect happens at a timescale slower than 1.3 ms. We attribute the spectral diffusion described here, and commonly observed on diamond color centers [31,32], to light-induced charge instabilities of lattice defects [33]. The measured value of  $F_{r.m.s} = 2.4$  MV/m corresponds to the electric field from a single charge 12 nm away. This distance is much smaller than the mean separation between nitrogen and boron impurities in the diamond substrate, which for a defect density of  $< 5$  ppb is expected to be  $> 100$  nm. It is instead likely related to lattice defects due to the Sn implantation [34]. Future work should study further the origin and timescale of charge noise on different color centers, including the role of ion implantation and nanofabrication.

To further investigate the residual broadening above the lifetime limit, we measure the linewidth shown by the emitter at smaller timescales. The results, obtained under

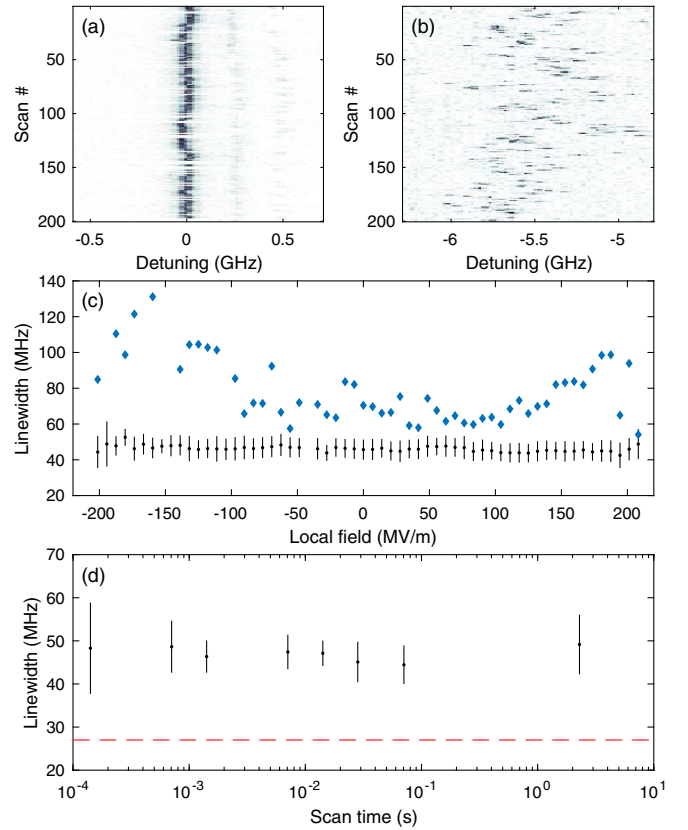


FIG. 4. Panel (a) and (b) show the SnV transition repeatedly probed over 1.3 ms, for an electric field of 0 MV/m and 250 MV/m respectively. (c) Black dots: Lorentzian linewidth observed in an individual scan, averaged over 200 repetitions. Blue diamonds: expected Voigt linewidth by combining the Lorentzian linewidth from a single scan and the Gaussian broadening from the standard deviation of the peak positions over the 200 repetitions. (d) Single-scan linewidth measured at 0 MV/m as a function of the laser scan time across the transition (black dots). The red dashed line shows the lifetime limited value.

zero bias, are shown in Fig. 4(d). We see no clear dependence on the laser scan time over the tested range, which span from 140  $\mu$ s to 2.3 s. Overall, the observed linewidth is consistently a factor of 1.7 above the lifetime limit. The residual broadening originates from processes occurring above 7 kHz. Unfortunately, this timescale is not accessible here due to the limited detected count rate. However, having confirmed that the diffusion due to the stochastic Stark shifts happens at a slower rate, we can exclude charge noise as a significant contributor to broadening. The power broadening induced by the probe laser is also negligible, so the deviation from the lifetime limited linewidth is likely due to residual interaction with the acoustic phonon bath [13,35].

The techniques used here proved very useful to understand the effect of charge noise on SnVs. As an additional example, we observed a linewidth narrowing effect on some SnV emitters at intermediate field values, detailed in Sec. 4 of the Supplemental Material [17]. We attribute this

to the suppression of spectral diffusion from the sweep-out of charge traps, which is commonly observed in other systems such as self-assembled quantum dots [36] and silicon carbide defects [37]. Second, we performed electric field-resolved spectroscopy on the 645 nm emission line, commonly observed in Sn-implanted diamond. As detailed in section 5 of the Supplemental Material [17], this reveals a linear Stark shift, indicating a permanent dipole moment that is not consistent with the SnV's inversion symmetry.

In conclusion, our measurements confirm the expected first-order insensitivity to electric fields and reveal suppressed second order effects on the SnV, which we quantified by the  $\Delta\mu$  and  $\Delta\alpha$  parameters reported in Fig. 3. Additionally, we use the emitter's linewidth to probe the local electric field noise by modulating its electric dipole, showing that spectral diffusion does not significantly contribute to the SnV residual broadening. We expect this technique to be broadly useful for characterizing local electric noise, from studies on quantum emitters [38] to cold atom systems [39] and superconducting qubits [40]. Our experiments also demonstrated the first Stark-shift control of a group IV-vacancy color center emission. Despite not offering the same tuning range as strain fields [10], this Stark shifting enables precise and easy-to-implement spectral tuning of group-IV centers. It is moreover compatible with high-speed modulation, as demanded in proposals for photon-photon logic gates [41,42]. Combined with large-scale integration of color centers on photonic circuits [11], it opens the path to scalable control of quantum memories in spin-photon quantum information processing systems.

L. D. acknowledge funding from the European Union's Horizon 2020 research and innovation program under the Marie Skłodowska-Curie grant agreement No. 840393. M. T. acknowledges support through the Army Research Laboratory ENIAC Distinguished Postdoctoral Fellowship. K. C. C. acknowledges funding support by the National Science Foundation Graduate Research Fellowships Program (GRFP) and the NSF STC Center for Integrated Quantum Materials (CIQM), NSF Grant No. DMR-1231319 and NSF Award No. 1839155. D. E. acknowledges further support by the MITRE Quantum Moonshot Program.

*Note added.*—During the writing of this manuscript we become aware of similar work investigating the use of single molecules for sensing charge fluctuations in GaP [43].

\* englund@mit.edu

† ldesanti@mit.edu

- [1] B. Hensen, H. Bernien, A. E. Dreaú, A. Reiserer, N. Kalb, M. S. Blok, J. Ruitenber, R. F. Vermeulen, R. N. Schouten, C. Abellán, W. Amaya, V. Pruneri, M. W. Mitchell,

- M. Markham, D. J. Twitchen, D. Elkouss, S. Wehner, T. H. Taminiau, and R. Hanson, Loophole-free Bell inequality violation using electron spins separated by 1.3 kilometres, *Nature (London)* **526**, 682 (2015).
- [2] L. Childress, M. V. Gurudev Dutt, J. M. Taylor, A. S. Zibrov, F. Jelezko, J. Wrachtrup, P. R. Hemmer, and M. D. Lukin, Coherent dynamics of coupled electron and nuclear spin qubits in diamond, *Science* **314**, 281 (2006).
- [3] P. C. Humphreys, N. Kalb, J. P. Morits, R. N. Schouten, R. F. Vermeulen, D. J. Twitchen, M. Markham, and R. Hanson, Deterministic delivery of remote entanglement on a quantum network, *Nature (London)* **558**, 268 (2018).
- [4] A. Gruber, A. Dräbenstedt, C. Tietz, L. Fleury, J. Wrachtrup, and C. Von Borczyskowski, Scanning confocal optical microscopy and magnetic resonance on single defect centers, *Science* **276**, 2012 (1997).
- [5] A. Faraon, C. Santori, Z. Huang, V. M. Acosta, and R. G. Beausoleil, Coupling of Nitrogen-Vacancy Centers to Photonic Crystal Cavities in Monocrystalline Diamond, *Phys. Rev. Lett.* **109**, 033604 (2012).
- [6] L. Li, T. Schröder, E. H. Chen, M. Walsh, I. Bayn, J. Goldstein, O. Gaathon, M. E. Trusheim, M. Lu, J. Mower, M. Cotlet, M. L. Markham, D. J. Twitchen, and D. Englund, Coherent spin control of a nanocavity-enhanced qubit in diamond, *Nat. Commun.* **6**, 6173 (2015).
- [7] R. E. Evans, A. Sipahigil, D. D. Sukachev, A. S. Zibrov, and M. D. Lukin, Narrow-Linewidth Homogeneous Optical Emitters in Diamond Nanostructures via Silicon Ion Implantation, *Phys. Rev. Applied* **5**, 044010 (2016).
- [8] G. Thiering and A. Gali, Ab Initio Magneto-Optical Spectrum of Group-IV Vacancy Color Centers in Diamond, *Phys. Rev. X* **8**, 021063 (2018).
- [9] R. E. Evans, M. K. Bhaskar, D. D. Sukachev, C. T. Nguyen, A. Sipahigil, M. J. Burek, B. Machielse, G. H. Zhang, A. S. Zibrov, E. Bielejec, H. Park, M. Lončar, and M. D. Lukin, Photon-mediated interactions between quantum emitters in a diamond nanocavity, *Science* **362**, 662 (2018).
- [10] B. MacHielse, S. Bogdanovic, S. Meesala, S. Gauthier, M. J. Burek, G. Joe, M. Chalupnik, Y. I. Sohn, J. Holzgrafe, R. E. Evans, C. Chia, H. Atikian, M. K. Bhaskar, D. D. Sukachev, L. Shao, S. Maity, M. D. Lukin, and M. Lončar, Quantum Interference of Electromechanically Stabilized Emitters in Nanophotonic Devices, *Phys. Rev. X* **9**, 031022 (2019).
- [11] N. H. Wan, T. J. Lu, K. C. Chen, M. P. Walsh, M. E. Trusheim, L. De Santis, E. A. Bersin, I. B. Harris, S. L. Mouradian, I. R. Christen, E. S. Bielejec, and D. Englund, Large-scale integration of artificial atoms in hybrid photonic circuits, *Nature (London)* **583**, 226 (2020).
- [12] U. Wahl, J. G. Correia, R. Villarreal, E. Bourgeois, M. Gulka, M. Nesládek, A. Vantomme, and L. M. Pereira, Direct Structural Identification and Quantification of the Split-Vacancy Configuration for Implanted Sn in Diamond, *Phys. Rev. Lett.* **125**, 045301 (2020).
- [13] J. Görlitz, D. Herrmann, G. Thiering, P. Fuchs, M. Gandil, T. Iwasaki, T. Taniguchi, M. Kieschnick, J. Meijer, M. Hatano, A. Gali, and C. Becher, Spectroscopic investigations of negatively charged tin-vacancy centres in diamond, *New J. Phys.* **22**, 013048 (2020).

- [14] A. E. Rugar, H. Lu, C. Dory, S. Sun, P. J. McQuade, Z. X. Shen, N. A. Melosh, and J. Vučković, Generation of tin-vacancy centers in diamond via shallow ion implantation and subsequent diamond overgrowth, *Nano Lett.* **20**, 1614 (2020).
- [15] T. Iwasaki, Y. Miyamoto, T. Taniguchi, P. Siyushev, M. H. Metsch, F. Jelezko, and M. Hatano, Tin-Vacancy Quantum Emitters in Diamond, *Phys. Rev. Lett.* **119**, 253601 (2017).
- [16] M. E. Trusheim *et al.*, Transform-Limited Photons from a Coherent Tin-Vacancy Spin in Diamond, *Phys. Rev. Lett.* **124**, 023602 (2020).
- [17] See Supplemental Material at <http://link.aps.org/supplemental/10.1103/PhysRevLett.127.147402> for details on sample fabrication and experimental procedures, as well as extended data on the Stark shift of SnV emitters.
- [18] M. Bertolotti, *Masers and Lasers: An Historical Approach* (Adam Hilger, Bristol, 2015), pp. 108–161.
- [19] D. M. Bishop, Polarizability and hyperpolarizability of atoms and ions, *Theor. Comput. Chem.* **6**, 129 (1999).
- [20] A. D. Buckingham, Permanent and induced molecular moments and long-range intermolecular forces, in *Advances in Chemical Physics*, 1967 (John Wiley and Sons, Ltd, New York, 2007), pp. 107–142.
- [21] T. C. Choy, *Effective Medium Theory: Principles and Applications* (Oxford University Press, New York, 2015).
- [22] F. Grazioso, B. R. Patton, P. Delaney, M. L. Markham, D. J. Twitchen, and J. M. Smith, Measurement of the full stress tensor in a crystal using photoluminescence from point defects: The example of nitrogen vacancy centers in diamond, *Appl. Phys. Lett.* **103**, 101905 (2013).
- [23] M. Bauer and L. Kador, Electric-field effects of two-level systems observed with single-molecule spectroscopy, *J. Chem. Phys.* **118**, 9069 (2003).
- [24] I. Gerhardt, G. Wrigge, and V. Sandoghdar, Control and imaging of single-molecule spectral dynamics using a nano-electrode, *Mol. Phys.* **107**, 1975 (2009).
- [25] P. Tamarat, T. Gaebel, J. R. Rabeau, M. Khan, A. D. Greentree, H. Wilson, L. C. Hollenberg, S. Praver, P. Hemmer, F. Jelezko, and J. Wrachtrup, Stark Shift Control of Single Optical Centers in Diamond, *Phys. Rev. Lett.* **97**, 083002 (2006).
- [26] P. Tamarat, N. B. Manson, J. P. Harrison, R. L. McMurtrie, A. Nizovtsev, C. Santori, R. G. Beausoleil, P. Neumann, T. Gaebel, F. Jelezko, P. Hemmer, and J. Wrachtrup, Spin-flip and spin-conserving optical transitions of the nitrogen-vacancy centre in diamond, *New J. Phys.* **10**, 045004 (2008).
- [27] T. Y. Latychevskaia, A. Renn, and U. P. Wild, Higher-order Stark effect on single-molecules, *Chem. Phys.* **282**, 109 (2002).
- [28] T. Haseyama, K. Kominato, M. Shibata, S. Yamada, T. Saida, T. Nakura, Y. Kishimoto, M. Tada, I. Ogawa, H. Funahashi, K. Yamamoto, and S. Matsuki, Second- and fourth-order Stark shifts and their principal-quantum-number dependence in high Rydberg states of  $85\text{Rb}$ , *Phys. Lett. A* **317**, 450 (2003).
- [29] E. E. Whiting, An empirical approximation to the Voigt profile, *J. Quant. Spectrosc. Radiat. Transfer* **8**, 1379 (1968).
- [30] A. V. Kuhlmann, J. Houel, A. Ludwig, L. Greuter, D. Reuter, A. D. Wieck, M. Poggio, and R. J. Warburton, Charge noise and spin noise in a semiconductor quantum device, *Nat. Phys.* **9**, 570 (2013).
- [31] S. B. Van Dam, M. Walsh, M. J. Degen, E. Bersin, S. L. Mouradian, A. Galiullin, M. Ruf, M. Ijspeert, T. H. Taminiou, R. Hanson, and D. R. Englund, Optical coherence of diamond nitrogen-vacancy centers formed by ion implantation and annealing, *Phys. Rev. B* **99**, 161203(R) (2019).
- [32] C. Santori, P. E. Barclay, K. M. Fu, R. G. Beausoleil, S. Spillane, and M. Fisch, Nanophotonics for quantum optics using nitrogen-vacancy centers in diamond, *Nanotechnology* **21**, 274008 (2010).
- [33] J. Wolters, N. Sadzak, A. W. Schell, T. Schröder, and O. Benson, Measurement of the Ultrafast Spectral Diffusion of the Optical Transition of Nitrogen Vacancy Centers in Nano-Size Diamond Using Correlation Interferometry, *Phys. Rev. Lett.* **110**, 027401 (2013).
- [34] T. Lühmann, J. Küpper, S. Dietel, R. Staacke, J. Meijer, and S. Pezzagna, Charge-state tuning of single SnV centers in diamond, *ACS Photonics* **7**, 3376 (2020).
- [35] K. D. Jahnke, A. Sipahigil, J. M. Binder, M. W. Doherty, M. Metsch, L. J. Rogers, N. B. Manson, M. D. Lukin, and F. Jelezko, Electron-phonon processes of the silicon-vacancy centre in diamond, *New J. Phys.* **17**, 043011 (2015).
- [36] A. V. Kuhlmann, J. H. Prechtel, J. Houel, A. Ludwig, D. Reuter, A. D. Wieck, and R. J. Warburton, Transform-limited single photons from a single quantum dot, *Nat. Commun.* **6**, 8204 (2015).
- [37] C. P. Anderson, A. Bourassa, K. C. Miao, G. Wolfowicz, P. J. Mintun, A. L. Crook, H. Abe, J. Ul Hassan, N. T. Son, T. Ohshima, and D. D. Awschalom, Electrical and optical control of single spins integrated in scalable semiconductor devices, *Science* **366**, 1225 (2019).
- [38] J. Houel, A. V. Kuhlmann, L. Greuter, F. Xue, M. Poggio, R. J. Warburton, B. D. Gerardot, P. A. Dalgarno, A. Badolato, P. M. Petroff, A. Ludwig, D. Reuter, and A. D. Wieck, Probing Single-Charge Fluctuations at a GaAs/AlAs Interface Using Laser Spectroscopy on a Nearby InGaAs Quantum Dot, *Phys. Rev. Lett.* **108**, 107401 (2012).
- [39] J. A. Sedlacek, A. Greene, J. Stuart, R. McConnell, C. D. Bruzewicz, J. M. Sage, and J. Chiaverini, Distance scaling of electric-field noise in a surface-electrode ion trap, *Phys. Rev. A* **97**, 020302 (2018).
- [40] P. V. Klimov *et al.*, Fluctuations of Energy-Relaxation Times in Superconducting Qubits, *Phys. Rev. Lett.* **121**, 090502 (2018).
- [41] M. Heuck, K. Jacobs, and D. R. Englund, Photon-photon interactions in dynamically coupled cavities, *Phys. Rev. A* **101**, 042322 (2020).
- [42] R. Trivedi, A. White, S. Fan, and J. Vučković, Analytic and geometric properties of scattering from periodically modulated quantum-optical systems, *Phys. Rev. A* **102**, 033707 (2020).
- [43] A. Shkarin, D. Rattenbacher, J. Renger, S. Hönl, T. Utikal, P. Seidler, S. Götzinger, and V. Sandoghdar, Nanoscopic Charge Fluctuations in a Gallium Phosphide Waveguide Measured by Single Molecules, *Phys. Rev. Lett.* **126**, 133602 (2021).